ELECTRON IRRADIATION DAMAGE IN NiO

M.I. BUCKETT and L.D. MARKS

Center for Surface Radiation Damage Studies and Department of Materials Science and Engineering, Northwestern University, Evanston, IL 60208, USA

The electron irradiation behavior of NiO has been systematically investigated in terms of beam energy and flux, crystal orientation, and surface environment, under both UHV (10^{-10} Torr) and non-UHV (10^{-7} Torr) conditions. The microscope vacuum was determined to be a major factor in the type of surface damage observed. Under UHV conditions, NiO showed only ballistic surface erosion. Under non-UHV conditions, electron-stimulated reactions occurred in competition with ballistic processes. In this case, the synergistic response of the material to both ionization and ballistic damage mechanisms generally resulted in more complicated surface structural changes and accelerated the erosion process. Reaction of the NiO surface with gaseous species in the microscope resulted in the formation of a Ni_3O_4 spinel phase. In the presence of reactive carbon, the NiO surface reduced to islands of metallic nickel. Encapsulation by a tenacious, graphitic carbon layer provided protection of the surface from electron irradiation damage.

1. Introduction

NiO surfaces have been extensively studied by conventional surface science techniques [1–4,28–30,33–42]; however observations remain inconclusive regarding electron irradiation effects such as electron-stimulated desorption (ESD) and electron-stimulated reaction (ESR). Conflicting investigations report both oxygen (O^+) ESD similar to that of the maximum valence transition metal (TM) oxides [1,2] as well as no oxygen loss [3,4]. Electron irradiation effects in oxide systems have also been investigated in the electron microscope, but not under UHV conditions [5–12]. For the maximum valence TM oxides, HREM results generally support the surface science findings of a strong tendency to undergo oxygen loss at the surface during electron irradiation [7–12]. For NiO, however, HREM investigations have not been conclusive [10,13–15]. We believe that this is largely due to variations in experimental conditions. HREM contributions to surface studies of ESD or ESR can only be considered valid if performed under surface science conditions or at least in controlled environments. With the development of UHV vacuum systems and better than

1.8 Å resolution instruments, high resolution electron microscopy (HREM) has only recently entered the surface science arena as a complementary technique for surface characterization [16–18]. As an example of the critical influence of microscope vacuum, we present the results of examining a NiO surface under conventional HREM conditions compared to examining the same surface under UHV conditions.

We have observed electron beam-induced structural changes occurring in-situ in the electron microscope under both UHV and non-UHV conditions. The dependence of these processes on electron beam energy, flux, and crystal orientation has also been investigated. Our results indicate that the NiO surface suffers only from ballistic knock-on damage in the UHV environment. Two specific beam-induced reactions have been observed under non-UHV conditions or in the presence of reactive surface species. First, a reaction occurs at the NiO surface which results in the formation of a Ni_3O_4 spinel phase. Secondly, in specimens where reactive carbon is present, a vigorous reduction reaction occurs which varies in extent from the formation of nickel islands to apparent melting. If, however, a graphitic carbon

contamination layer encapsulates the NiO surface, it remains stable for prolonged periods of exposure to the electron beam.

2. Experimental

NiO samples used for this study were high purity bulk single crystals provided by Argonne National Laboratory [19]. The composition of these crystals was $Ni_{1-x}O$, with x being 0.0001. TEM samples were prepared by crushing the bulk crystal with an agate mortar and pestle. Samples were both dry crushed, and crushed under high purity methanol. Essentially no difference was noted with these two preparation conditions; however a better particle size distribution was obtained with the wet crushing method. In this case, the suspension was ultrasonically mixed and a droplet of the solution was typically placed on a holey carbon film supported on a Cu grid. For the UHV experiments, a SiO support film was used. The UHV samples were baked in-situ at approximately 150°C for 12 h. The question of sample contamination from the agate mortar and pestle was evaluated by crushing some samples in nickel foil. Again, essentially no difference was noted with these two preparation techniques.

NiO profile surfaces were examined in a Hitachi H-9000 high resolution electron microscope with a vacuum of approximately 3×10^{-7} Torr and also in a Hitachi UHV H-9000 microscope with a vacuum of approximately 1.5×10^{-10} Torr, both operating at either 100 or 300 kV. Optimum particle sizes ranged from 5 to 10 μm in diameter and roughly 30 to 100 Å thick at the profile surface. The [001] and [110] crystal orientations were examined in detail. The [111] orientation was also examined, but was rarely seen and thus only diffraction and qualitative structural information could be obtained. For the remainder of the text, brackets [ ] will be used to indicate the crystallographic zone being described. The notation [zone]/(profile plane) will be used to indicate specific profile surfaces.

Each sample was irradiated by centering the focused electron beam at the specimen profile edge as shown in fig. 1. Two specific electron flux
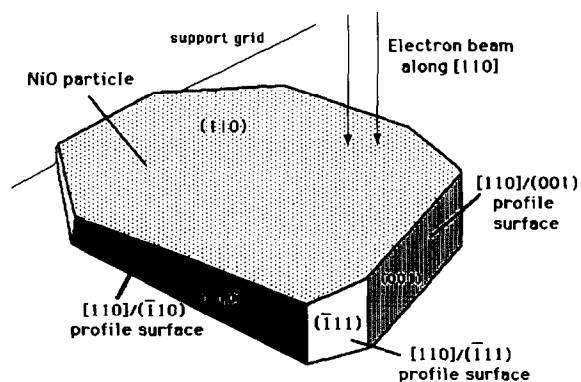

Fig. 1. Schematic diagram of the experimental set-up for a [110] zone orientation. Specific profile planes are indicated by [zone]/(profile plane) notation.

conditions, low and high, were used. In the low flux condition, a condensor aperture was inserted. For our microscope, this resulted in an electron flux of 10 A/cm², measured with a Faraday cage placed in the viewing chamber. In the high flux condition the condensor aperture was removed, resulting in an electron flux one order of magnitude higher. The incident electron energy dependence was determined by varying the operating voltage of the microscope.

In addition to conventional TEM recording, videotape and direct computer image acquisition were used to more accurately determine time evolution of events. Multislice image calculations of the profile surface were carried out and compared to experimental profile images, using the guidelines and considerations outlined in ref. [17].

3. Results

Damage processes in NiO fell into three categories: ballistic, surface-initiated oxidation to a Ni_3O_4 spinel phase, and surface-initiated reduction to metallic nickel. Ballistic damage was observed under all experimental conditions at 300 kV irradiation. Formation of the spinel phase was observed only in the non-UHV environment. Metallic nickel was observed only in the presence of soft or amorphous carbon. A summary of the results is presented in table 1.

Table 1
Summary of electron irradiation damage in NiO

(a) Electron energy = 300 keV, vacuum = 3×10^{-7} Torr (4×10^{-5} Pa)

Sample orientation	Clean		Reactive carbon present	
	High flux	Low flux	High flux	Low flux
[001]	Ballistic surface erosion, scarce traces of Ni_3O_4	Ballistic surface erosion, competing Ni_3O_4 formation	Spontaneous disintegration	Spontaneous reaction to form Ni islands, recrystallization, spontaneous disintegration
[110]	Ballistic erosion of surface, scarce traces of Ni_3O_4	Ballistic erosion of surface, competing Ni_3O_4 formation	Spontaneous disintegration	Spontaneous reaction to form Ni islands, recrystallization, spontaneous disintegration
[111]	–	Ballistic erosion of surface, competing Ni_3O_4 surface phase formation	–	–

(b) Electron energy = 100 keV, vacuum = 3×10^{-7} Torr (4×10^{-5} Pa)

Sample orientation	Clean		Reactive carbon present	
	High flux	Low flux	High flux	Low flux
[001]	–	–	Recrystallization, disintegration	–
[110]	–	Formation of Ni_3O_4 surface phase	–	–
[111]	–	–	Spontaneous disintegration	–

(c) Vacuum = 1.5×10^{-10} Torr (2×10^{-8} Pa)

Only ballistic knock-on damage was observed under UHV conditions in all cases

3.1. Ballistic damage

The most prevalent structural modification seen in NiO during electron irradiation was ballistic surface erosion. This type of knock-on damage was observed with 300 but not 100 kV irradiation, which is in agreement with previous studies [15]. In UHV, ballistic knock-on was the primary type of beam damage observed and could be easily monitored, presumably due to cleaner initial surfaces and the absence of a carbon encapsula-

tion layer [6]. A precise measurement of the ballistic sputtering threshold was made in the UHV microscope by incrementing the microscope voltage and irradiating at high flux for 8 to 10 h at each increment. The average value obtained by making a number of measurements in this way was 103 ± 3 keV, which corresponds to a maximum ballistic energy transfer of approximately 4.3 eV to nickel and 15.7 eV to oxygen atoms.

Under non-UHV conditions, surface erosion occurred at an appreciable rate only during high
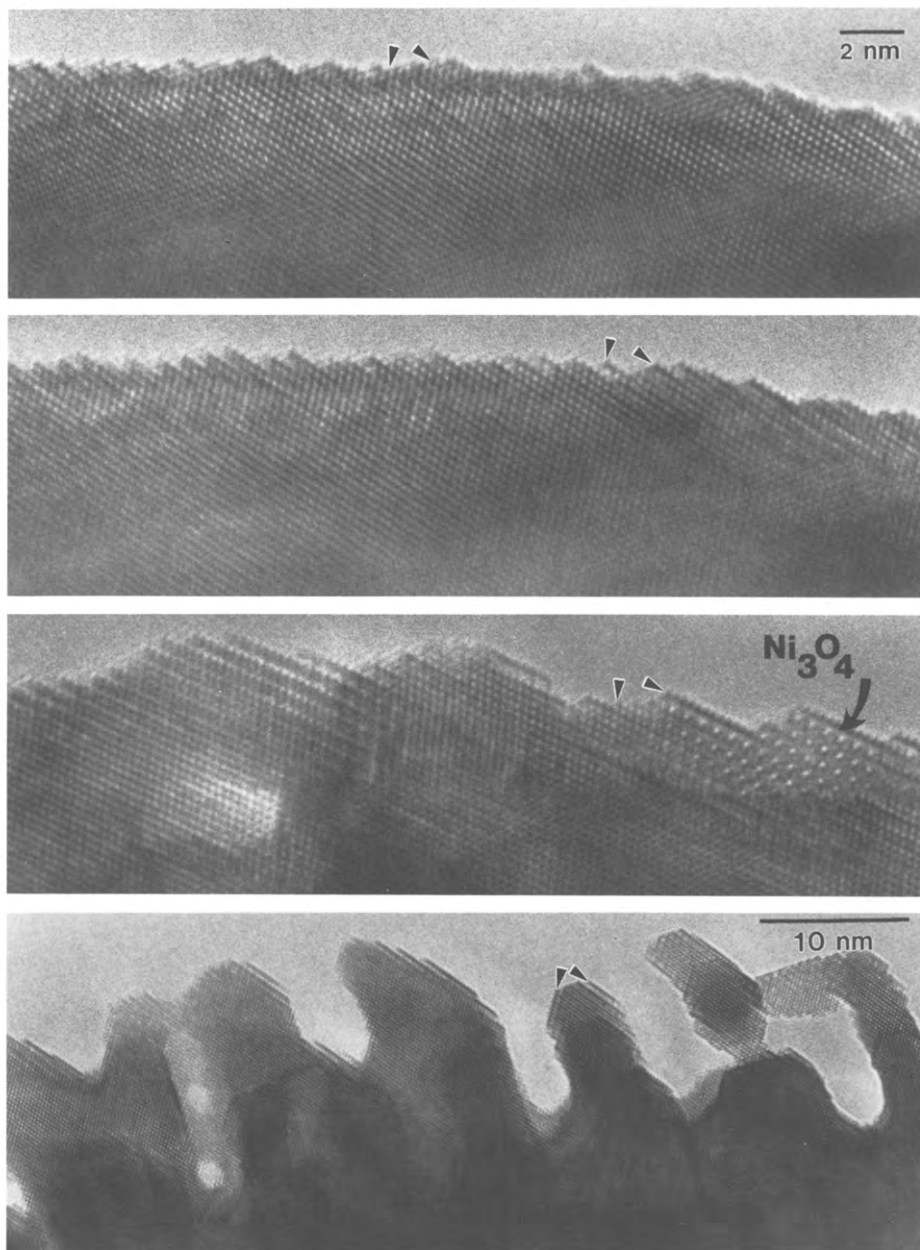
Fig. 2. Time evolution sequence showing electron irradiation damage in NiO [110] under non-UHV conditions. Triangular markers point to (111) profile planes. (a) Initial surface, (b) after 10 min of high flux irradiation, (111) faceting is evident, (c) after 60 min of high flux irradiation, areas of Ni_3O_4 are evident, (d) after 180 min of high flux irradiation, surface erosion has occurred anisotropically. Doubling of the surface (111) planes can still be seen.

flux irradiation. Ballistic surface erosion appeared to be anisotropic in this case. Shown in fig. 2 is a NiO particle in the [110] orientation, supported directly on a Cu grid (no carbon film), and irradiated under high flux in a vacuum of 3×10^{-7} Torr at 300 kV. The [110]/(110) and [110]/(001) pro-
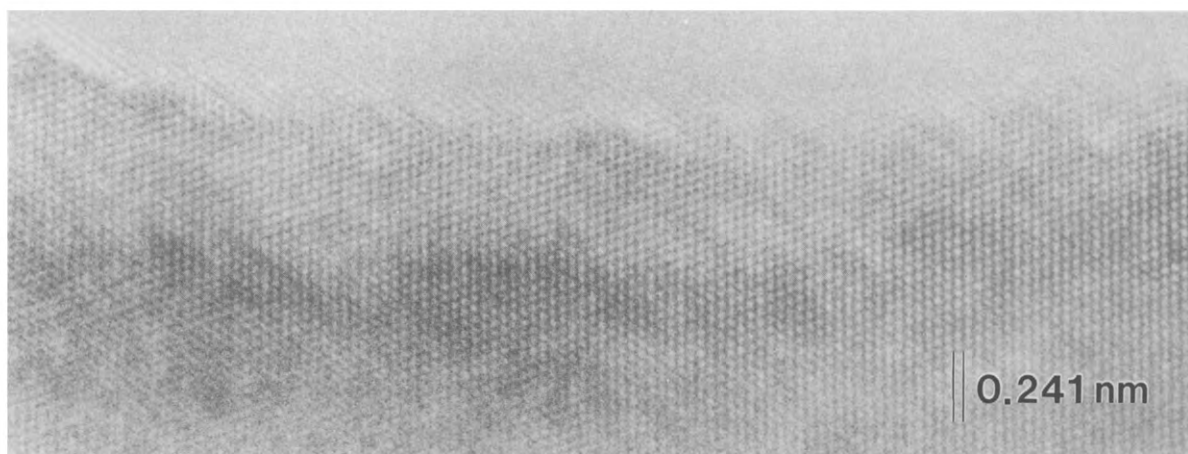
Fig. 3. NiO [110] after 120 min of low flux irradiation in UHV. Neither faceting nor doubling of the surface (111) profile planes are evident.

file surfaces were generally found to be unstable. These surfaces rapidly reoriented to [110]/(111) microfacets and erosion progressed along these facets preferentially. (111) facets were typically observed in NiO, apparently stable in the electron beam. A doubling of the surface [110]/(111) plane spacing also appeared very early on and was present throughout the irradiation (see fig. 2d). This surface characteristic was identified as a precursor to the Ni_3O_4 spinel phase and is described in detail in the next section. At low flux irradiation, transformation to the spinel phase was extensive. At high flux, it was observed only during early stages (fig. 2c), eventually being taken over by surface erosion with further exposure (fig. 2d). Neither a doubling of the [110]/(111) planes at the surface nor facets were observed under UHV conditions (fig. 3).

The NiO [001] orientation (fig. 4) showed similar surface erosion behavior. Ballistic damage, however, did not appear to be as highly anisotropic and damage rates were slower compared to the [110] orientation. Comparison of experimental to calculated images showed the surface to be a simple bulk termination as has been reported in the surface science literature [20,21].

3.2. Surface-initiated oxidation of Ni

In competition with ballistic knock-on damage, the surface-initiated nucleation of a Ni_3O_4 spinel phase was observed under non-UHV conditions (fig. 5). The spinel phase was identified from diffraction data and from through focal series comparison of experimental to simulated images. Selected area diffraction in three different orientations (fig. 6) showed the spinel structure to have a cube–cube orientation relationship and exactly double the NiO unit cell spacing. This beam-induced phase transformation to a spinel phase has also been observed in the CoO, MnO, and FeO systems, where the M_3O_4 type spinel structure is an equilibrium phase. In these cases, however, the spinel structures indexed to the known lattice parameters, not a simple doubling of the monoxide unit cell [22].

The Ni_3O_4 phase transformation readily occurred at both 100 and 300 kV and was observed to be reversible. That is, this phase slowly reverted to the original NiO structure when the electron beam was removed. This was contrary to the observations for CoO, MnO, and FeO, where the spinel phase remained after the beam was removed. Neither significant mass loss nor volume expansion were apparent, however surface rearrangement was clearly observed. A threshold flux of approximately 3 A/cm^2 was required for the onset of this phase transformation. With further increasing flux or longer exposure times, spinel formation was overshadowed by ballistic knock-on damage (see figs. 2a–2d). The early stages of this transformation were characterized
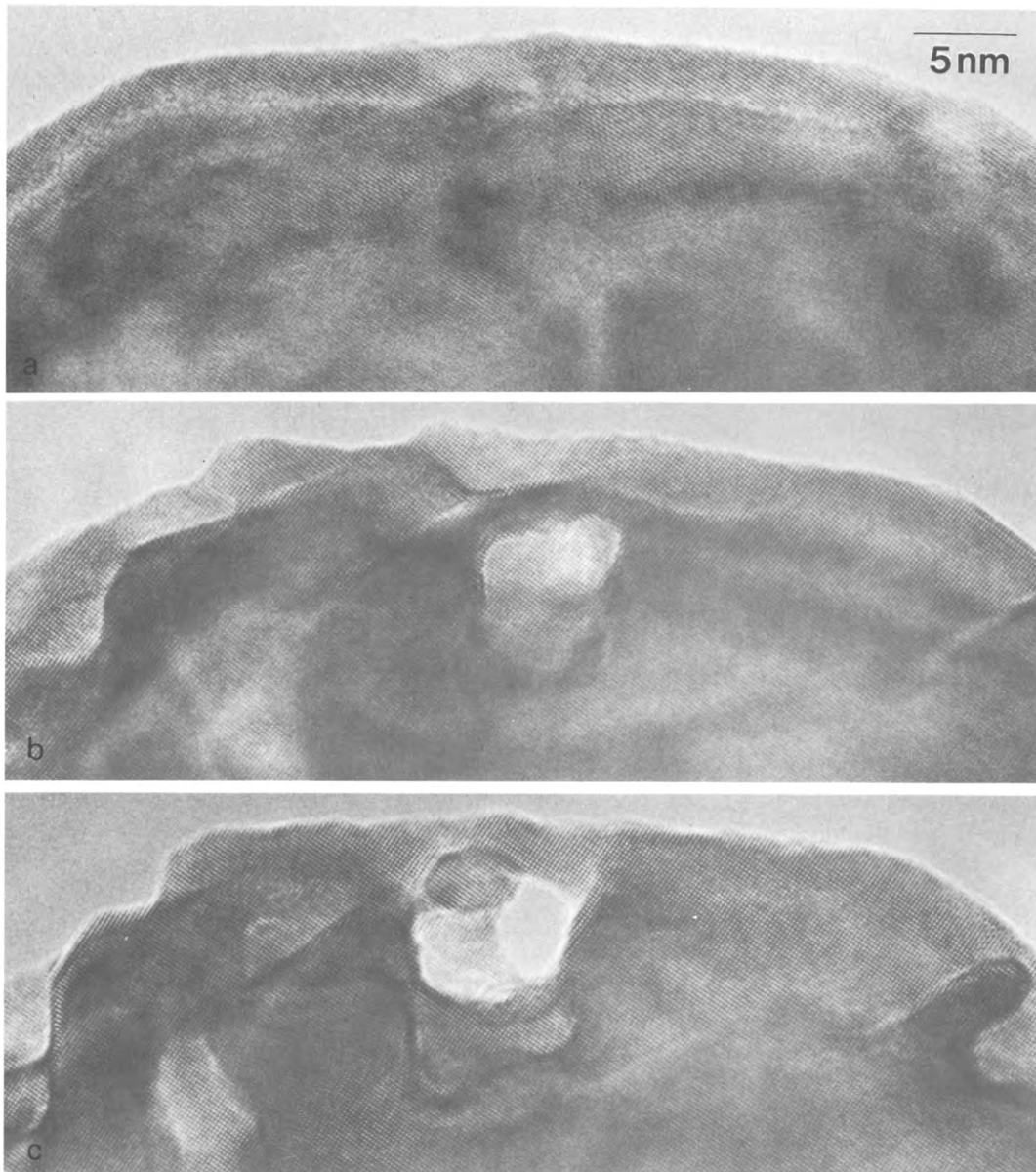
Fig. 4. Time evolution sequence of electron irradiation damage in NiO [001] under non-UHV conditions. (a) After 10 min of high flux irradiation (essentially unchanged from initial surface), (b) after 65 min of high flux irradiation, (c) after 90 min of high flux irradiation.

by a precursor state – the doubling of the surface (111) planes, most easily evident in the [110] orientation as seen in fig. 2d.

Growth of the spinel phase into the bulk behaved as a diffusion-controlled process. Progression of the growth front inward from the surface could be monitored layer-by-layer as shown in fig. 7. It was strongly orientation dependent. For example, diffusion paths along $\langle 112 \rangle$ directions inward from the [110]/(111) and [110]/(110) profile surfaces were preferred without exception. If one assumes that the propagation of the spinel phase
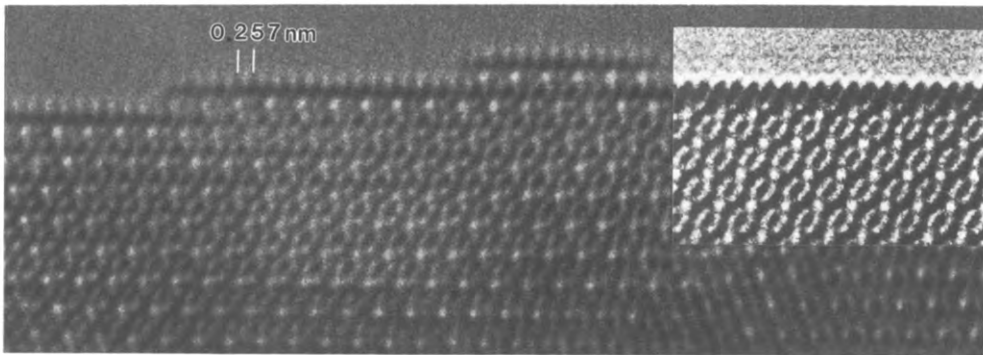
Fig. 5. (111) profile surface where the Ni_3O_4 spinel phase has formed. The calculated image is inset. (Defocus = -440 Å.) This best-fit calculated image includes 2 monolayers of NiO at the (111) profile surface.

into the bulk is via point defect migration (perhaps Ni^{3+}), the mobile species is nickel [23,24], and the ionic radius of Ni^{3+} is approximately 0.58 Å [25], growth would be limited to diffusion paths along the Ni(111) layers. This type of layer-by-layer growth corresponds to the experimental observations. From a number of time evolution sequences, an average diffusion coefficient was determined to be approximately 4×10^{-15} cm^2/s by estimating the thickness and shape of the crystal from the through focal series image simulations

and assuming the diffusing species are Ni^{3+} defects propagating along the (111) layers.

Further support of this conclusion is that the structural transformation of NiO (rocksalt structure) to Ni_3O_4 (spinel structure) progressed almost entirely on the nickel sublattice as evidenced by dynamic observation of growth along the (111) layers. If the assumption is that a nickel vacancy is created, formation of Ni_3O_4 spinel from four formula units of the parent NiO requires only that one half of the nickel go from Ni^{2+} to Ni^{3+}
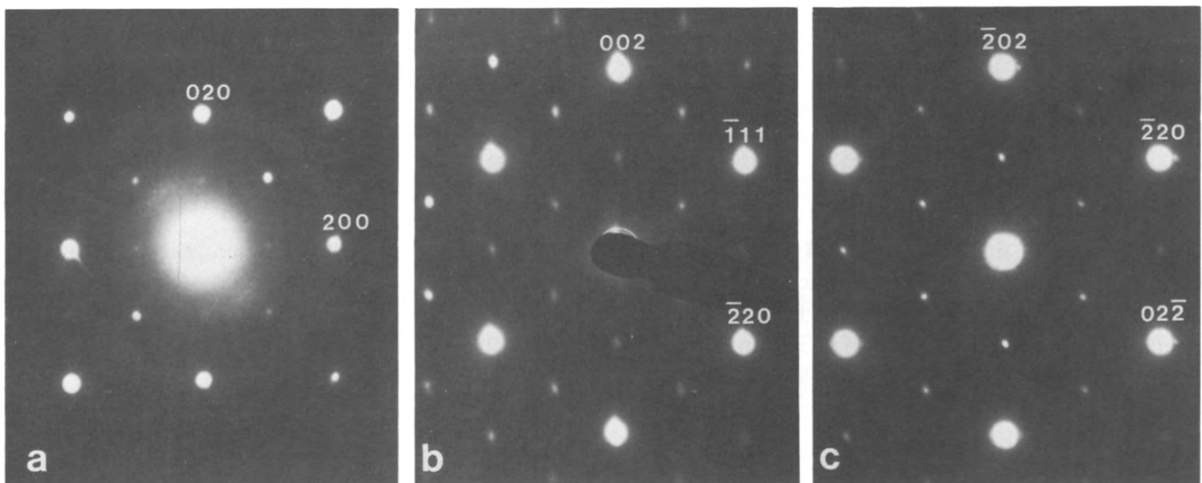

Fig. 6. Electron diffraction patterns indicate that Ni_3O_4 spinel forms with a cube–cube epitaxy to the parent NiO. (a) [001] orientation, (b) [110] orientation, (c) [111] orientation.
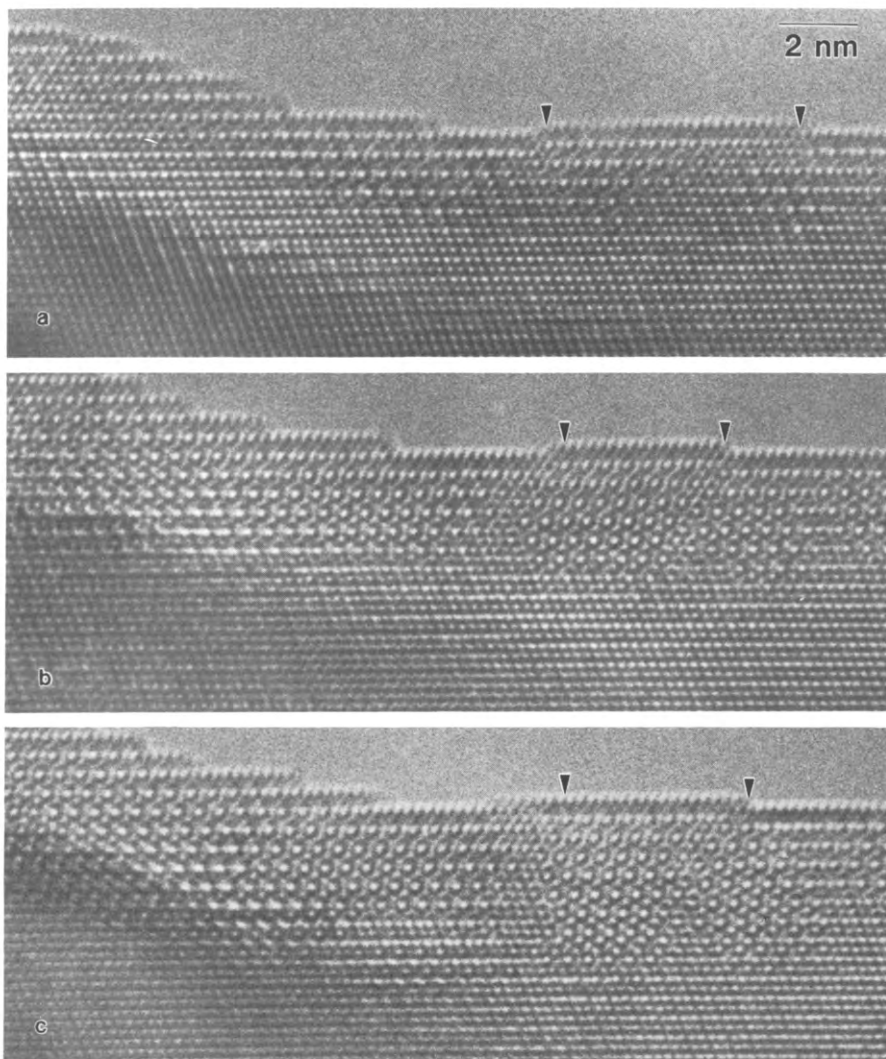
Fig. 7. Time evolution sequence showing diffusion of the spinel into the bulk. Arrows at left mark a fixed position in the sample. Arrows at right illustrate the rearrangement occurring at the surface. Preferential growth of the spinel phase along (111) planes is evident. (a) After 5 min low flux irradiation, (b) after 20 min, (c) after 30 min.

charge states and that one fourth of the nickel on octahedral sites move into tetrahedral sites. If Ni_3O_4 is an inverse spinel, then the nickel on tetrahedral sites are Ni^{3+} ions. If it is a normal spinel, then the nickel on tetrahedral sites are Ni^{2+} ions. Consideration of ionic size and the fact that the inverse spinel is the more conductive of the two possible structures, a reasonable guess would be that the inverse spinel has formed. It should be noted, however, that HREM image

simulation is not a sensitive enough technique to unambiguously differentiate between the two structures. The inverse spinel structure was used for the image calculations.

3.3. Surface-initiated reduction of Ni

In the presence of soft carbon (e.g. contamination on the surface or the carbon support), a spontaneous reaction occurred which resulted in
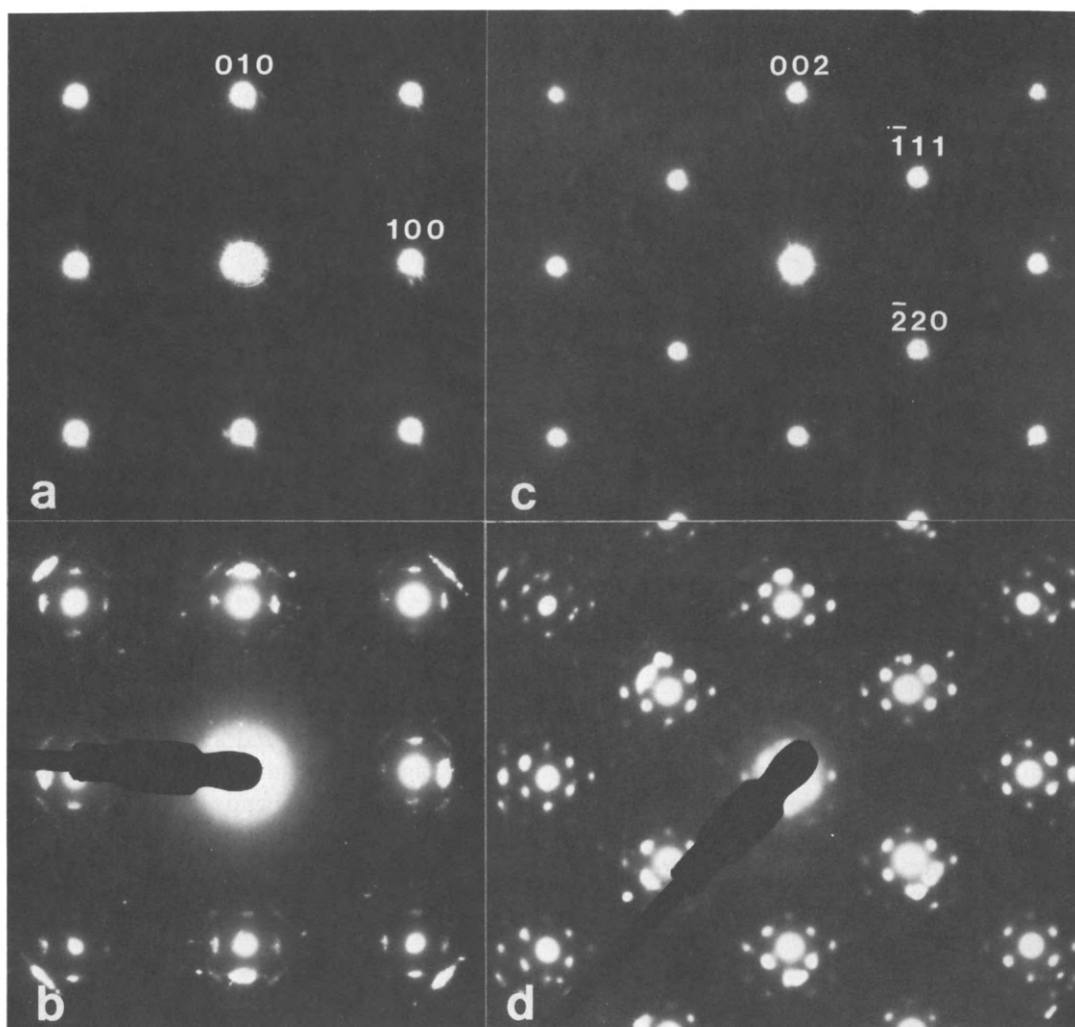
Fig. 8. Electron diffraction patterns before and after ESR to metallic nickel at the surface indicate that the nickel islands form with a cube–cube epitaxy to the parent NiO. (a) and (b) [001] orientation, (c) and (d) [110] orientation.

the reduction of the NiO surface to metallic nickel of cube–cube epitaxy (figs. 8 and 9). The influence of the carbonaceous species was verified by artificially evaporating a small amount of carbon onto NiO particles supported on a holey SiO film and Cu grid. The carbon "islands" were seen to disintegrate into the bulk, leaving behind metallic nickel. This reaction varied in extent (apparently due to the amount of reactive carbon present) from the formation of nickel islands to more extensive bulk structural changes such as recrystallization, complete disintegration, and/or apparent melting of the sample (fig. 10). It occurred more

vigorously at either higher electron fluxes or lower electron energies, characteristic of an electronic rather than a knock-on or thermal process. Similar findings have been reported in other microscopy investigations under various conditions [13–15]. In all cases, it appeared that the interaction of the electron beam and reactive carbonaceous species caused severe degradation of the NiO surface.

3.4. Graphitic carbon encapsulation layers

On occasion, a contamination layer ranging in thickness from 10 to 100 Å would form on the
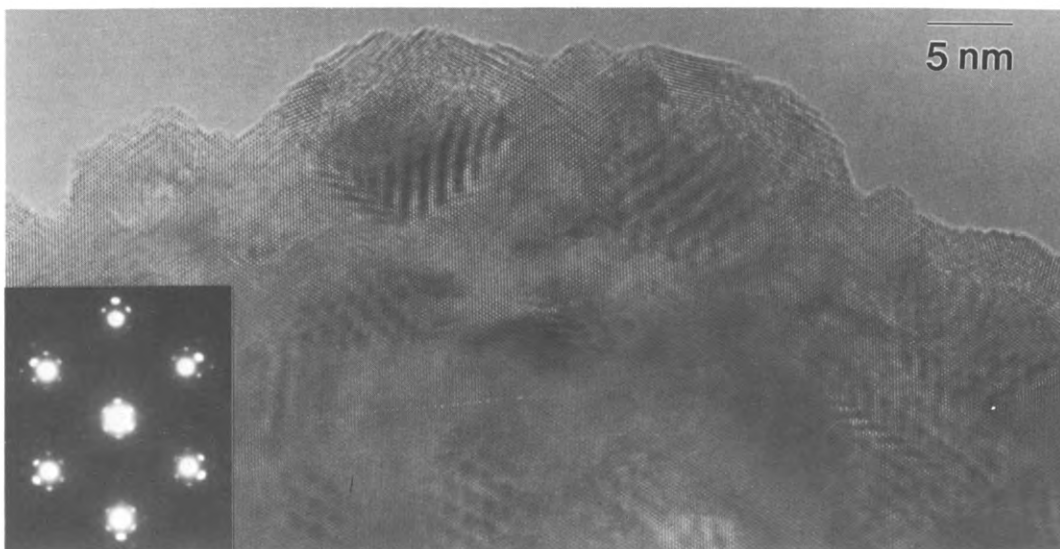
Fig. 9. HREM image of NiO after ESR in the presence of reactive carbon to form islands of metallic nickel at the surface.

surface of a specimen as shown in fig. 11. Thin contamination layers (≤ 10 Å) could usually be etched away with time by the electron beam [18]. Thicker, tenacious contamination layers were often identified as wholly or partially graphitized carbon, both very difficult to remove. Graphitic surface contamination is not uncommon in microscopy work, even though the exact conditions under which it forms are not well known [16]. (Nickel is also a known catalyst for the graphitization of carbon [26,27].) Samples encapsulated under graphitic layers were exceedingly resistent to radiation damage. Even under high flux irradiation, no evidence of radiation damage was observed in time periods exceeding 3 h for well-encapsulated layers, thus confirming the critical role of the surface.

4. Discussion

In summary, the primary electron irradiation damage process observed in NiO was ballistic surface erosion, which varied directly with both electron energy and flux. In the UHV environment, ballistic surface erosion was the only form of radiation damage observed. Neither surface relaxation nor faceting were observed and surface

erosion did not show a strong orientation dependence. In the non-UHV environment, surface erosion could be monitored at appreciable rates only during high flux irradiation at 300 kV, due to the presence of carbon encapsulation layers and competing surface reactions. Ballistic damage under these conditions was accelerated along certain directions in the crystal; an effect more pronounced in the [110] than in the [001] orientation. This would be an expected result. The crystal planes in the [110] orientation consist of alternate (111) columns of nickel and oxygen parallel to the beam, a more favorable orientation for ballistic knock-on effects, rather than columns of mixed atoms. However, similar behavior was not observed under UHV conditions. The formation of the spinel phase may be contributing to accelerated surface erosion along preferred orientations under non-UHV conditions.

It was further determined that the Ni_3O_4 spinel transformation was a surface-initiated reaction via interaction with the local environment rather than a damage mechanism producing a nickel deficiency within the sample itself for the following reasons: (1) Neither the spinel phase nor its precursor state formed in specimens under UHV conditions. Insertion of the same specimens into a non-UHV microscope, however, resulted in char-
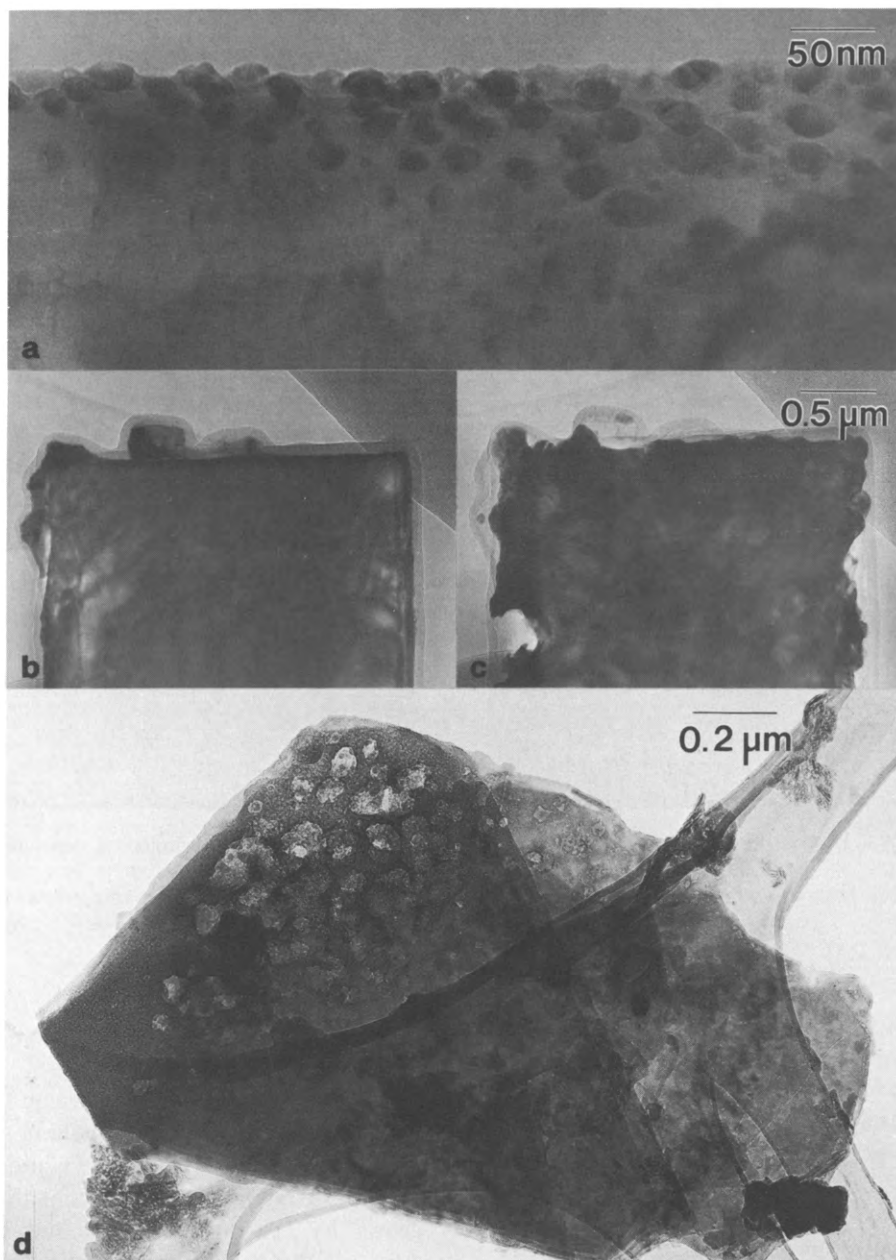
Fig. 10. Varying degrees of structural damage after ESR in the presence of reactive carbon. All reactions occurred within seconds of exposure to the electron beam. (a) Metallic nickel islands form during low flux irradiation at 300 kV, (b) before, and (c) after ESR during high flux irradiation at 300 kV, (d) complete disintegration after high flux irradiation at 100 kV.

acteristic spinel formation. (2) No evidence of bulk-initiated damage was observed under any conditions. (3) Nucleation of the spinel occurred preferably at a high energy surface site – a kink or step, or a NiO(111) facet. The spinel phase also did not form when the surface was encapsulated with a graphitic carbon layer (see section 3.4) under non-UHV conditions. For example, shown
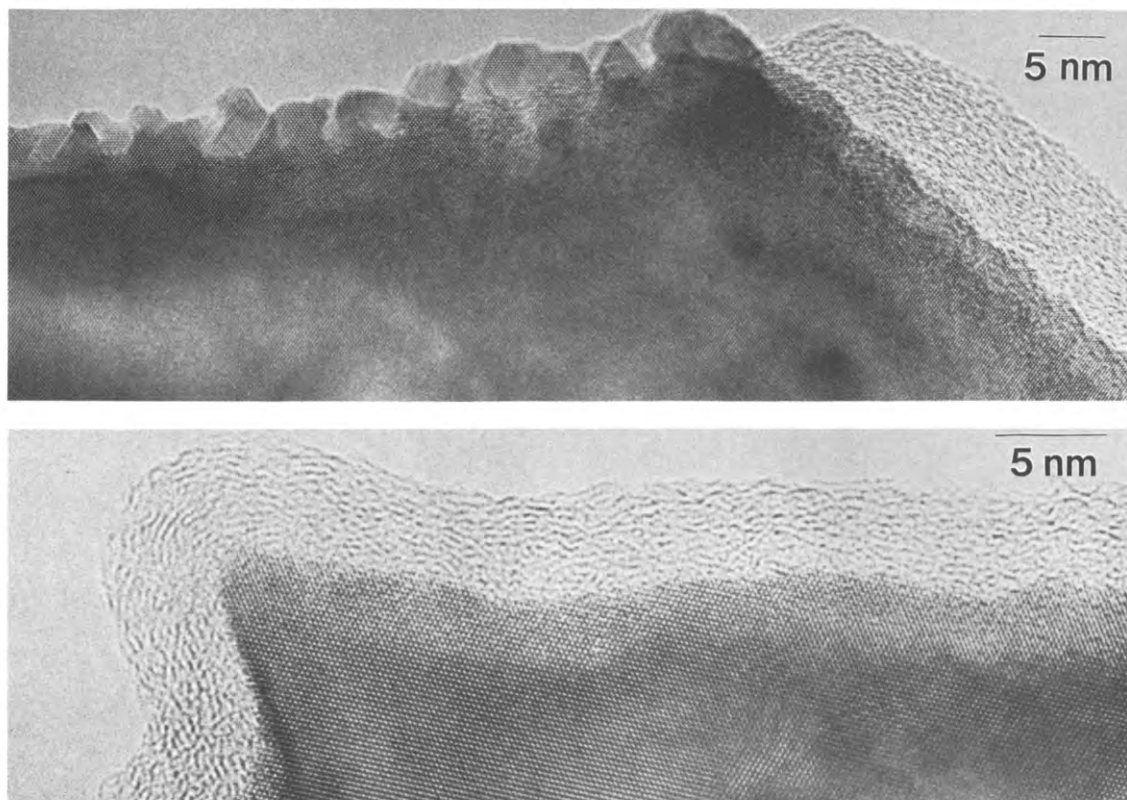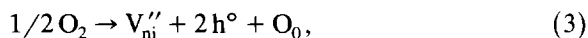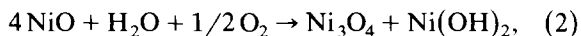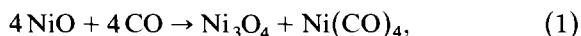
Fig. 11. Encapsulation by a graphitic carbon layer provided protection of the surface against prolonged exposure to both low and high flux electron irradiation. (a) Partially graphitized layer covers only part of surface. Exposed areas were seen to nucleate the spinel phase and with time, showed extensive ballistic surface erosion. (b) Partially graphitized layer encapsulates the entire surface. No surface degradation was evident during the 120 min of observation.

in fig. 8 is a NiO surface only partially encapsulated by a graphitic layer. In the encapsulated regions, no structural changes were observed. However, exposed surfaces showed the characteristic precursor to spinel formation within minutes of exposure to the electron beam and anisotropic ballistic damage with further time. It can only be concluded that the surface is undergoing an electron beam-stimulated interaction with some gaseous component in the microscope. The primarily components of the residual gas in the microscope are CO, CO_2, H_2O, N_2 and O_2. Reaction of these species with the NiO surface may lead to the formation of Ni_3O_4, for example:

$$4NiO + 4CO \rightarrow Ni_3O_4 + Ni(CO)_4, \quad (1)$$

$$4NiO + H_2O + 1/2O_2 \rightarrow Ni_3O_4 + Ni(OH)_2, \quad (2)$$

$$1/2O_2 \rightarrow V_{ni}'' + 2h^\circ + O_0, \quad (3)$$

$$4NiO \rightarrow Ni + Ni_3O_4. \quad (4)$$

The chemisorption of oxygen (reaction (3)), would require a significant volume increase. This was observed in the CoO, MnO, and FeO systems; but not in NiO – indicating that the spinel phase grows by rearrangement of the previous NiO structure not by addition of atoms to the surface. In addition, the phase transformation was reversible; therefore significant mass loss cannot be occurring (with the exception of species at the surface – creation of point defects which diffuse into the bulk at a rate we are able to monitor). One possible mechanism is via reaction (or adsorption) of gaseous species with nickel surface atoms at a step, kink, or [110]/(111) nickel facet, and subsequent electron-stimulated desorption of the reac-

tion product (e.g. reactions (1) or (2)). Another possibility would be a surface catalyzed redox reaction similar to the decomposition of wüstite (reaction (4)). In all cases, the driving force for the reaction appears to be the radiation-induced displacement of nickel site defects from octahedral sites into tetrahedral sites.

Doubling of the NiO lattice parameter [28,29] and precipitation of a defect spinel-type structure [25,30] have been previously recorded in the literature under different conditions than have been reported here. Shimomura et al. [25], reported that the structure of ferromagnetic (and later corrected to ferrimagnetic) NiO crystals prepared by the flame fusion method and analyzed by X-ray diffraction was a defect tetragonal structure belonging to I4$_1$/amd (D$_{4h}^{19}$). We have investigated this possibility using the ferrimagnetic structure data as a basis for image simulations. Under no conditions did the calculated images compare with the experimental images, thus ruling out antiferromagnetic NiO in our case. The structure determined by Shimomura et al., was later modified by Katada et al. [30], who observed temperatures of 1400–1600°C in air. Using electron diffraction as well as the X-ray data of ref. [25], they corrected the original structural determination to that of a deformed spinel-type based on the Fd3m-O$_h^7$ space group. They also observed the precipitates to generally have a regular octahedron shape with (111) face planes. This data correlates well with our observations. Katada et al., however, were unable to account for the large nickel deficiency required for complete transformation to the Ni$_3$O$_4$ composition.

The question of temperature rise in TEM specimens is always a concern. The theoretical temperature rise in TEM specimens can be estimated based on a model from Gale and Hale [31] and Fisher [32]. Using the worst case scenario of high flux (6×10^{20} e/cm^2/s) in a 1 μm thick sample, the theoretical temperature rise in NiO was calculated to be under 100°C, which is well under the 1400–1600°C required for the precipitation observed by Katada et al. In addition, the spinel transformation we observed was reversible. Spinel transformation in our case does not appear to be a thermally stimulated process (even though the resulting structure may be similar).

LEED studies [28,29] have reported on the appearance of half-order diffraction spots which were interpreted to result from spin ordering in antiferromagnetic NiO. These, however, were observed only below the Néel temperature (252°C) in UHV and at electron energies below 100 eV. The positions of the fractional order beams are believed to be due to a magnetic cell in antiferromagnetic NiO having double the unit cell spacing as the chemical cell and not phase transformation.

We conclude that under non-UHV microscope conditions, changes in the electronic structure are occurring at the surface of NiO which lead to the formation of Ni^{3+} defects on the nickel sublattice, in agreement with the surface science literature. This conclusion differs only in the determination of the resulting Ni$_3$O$_4$ spinel structure. Both the anomalous behavior of the O$^+$ yield during oxygen exposure of both nickel and NiO surfaces using ESID and AES techniques [2,4,33] and the appearance of Ni^{3+} on the surface of NiO using chemical shift information [34–38] have been reported in the surface science literature. These combined results were interpreted as the formation of Ni$_2$O$_3$ [34–36] during the early stages of the oxidation process, although no structural evidence for the formation of this phase has been reported. It has been proposed that the Ni$_2$O$_3$ phase may exist at low temperatures [39–41], with NiO being the favorable high temperature structure. Neither Ni$_2$O$_3$ nor Ni$_3$O$_4$ are known stable oxide structures in the NiO system, however the spinel phase is an equilibrium low temperature structure in related systems such as CoO, MnO, and FeO. As stated earlier, we have observed beam-induced spinel formation in both CoO and MnO, with FeO currently under investigation. From these observations, we predict that the surface oxidation of NiO seen in previous surface studies is due to the same Ni$_3$O$_4$ phase we observe rather than to Ni$_2$O$_3$ of undetermined structure.

Acknowledgements

K. Merkle for their helpful discussions, and Dr. K. Merkle for providing the NiO samples.

References

[1] H.C. Gerritsen, M.P. Bruijn, J. Verhoeven and M.J. van der Wiel, Surf. Sci. 139 (1984) 16.
[2] Wang Wen-hao and J. Verhoeven, Surf. Sci. 175 (1986) 325.
[3] M.L. Knotek and P.J. Feibelman, Phys. Rev. Lett. 40 (1978) 964.
[4] H. Niehus and W. Losch, Surf. Sci. 111 (1981) 344.
[5] L. Hobbs, in: Introduction to Analytical Electron Microscopy, Eds. J.J. Hren, J.I. Goldstein and D.C. Joy (Plenum, New York, 1979) p. 437.
[6] J. Strane, L.D. Marks, D.E. Luzzi, M.I. Buckett, J.P. Zhang and B.W. Wessels, Ultramicroscopy 25 (1988) 253.
[7] M.I. Buckett, J.W. Strane, D.E. Luzzi, J.P. Zhang, B.W. Wessels and L.D. Marks, Ultramicroscopy 29 (1989) 217.
[8] D.J. Smith and L.A. Bursill, Ultramicroscopy 17 (1985) 387.
[9] A.K. Petford, L.D. Marks and M. O'Keefe, Surf. Sci. 172 (1986) 496.
[10] D.J. Smith, L.A. Bursill and D.A. Jefferson, Surf. Sci. 175 (1986) 673.
[11] H. Fan and L.D. Marks, Ultramicroscopy 31 (1989) 357.
[12] S.R. Singh and L.D. Marks, Philos. Mag., in press.
[13] K.M. Ostyn and C.B. Carter, Electron Microsc. 2 (1982) 191.
[14] J. Liu and J.M. Cowley, Proc. 45th Annual Meeting of the EMSA (1987) p. 176.
[15] D.E. Luzzi, L.D. Marks, M. Buckett, J. Strane, B. Wessels and P. Stair, Mater. Res. Soc. Symp. Proc. 100 (1988) 635.
[16] L.D. Marks, Phys. Rev. Lett. 51 (1983) 1000.
[17] L.D. Marks, Surf. Sci. 139 (1984) 281.
[18] L.D. Marks and D.J. Smith, Surf. Sci. 143 (1984) 495.
[19] Samples provided courtesy of Dr. K. Merkle, Argonne National Laboratory.
[20] F.P. Netzer and M. Prutton, J. Phys. C 8 (1975) 2401.
[21] C.G. Kinniburgh and J.A. Walker, Surf. Sci. 63 (1977) 731.
[22] M.I. Buckett, Department of Materials Science and Engineering, Northwestern University, to be published.
[23] P. Kofstad, Nonstoichiometry, Diffusion, and Electrical Conductivity in Binary Metal Oxides (Wiley–Interscience, New York, 1972).
[24] N.L. Peterson and C.L. Wiley, J. Phys. Chem. Solids 46 (1985) 43.
[25] Y. Shimomura, M. Kojima and S. Saito, J. Phys. Soc. Jpn. 11 (1956) 1136.
[26] Y. Tamai, Y. Nishiyama and M. Takahashi, Carbon 6 (1968) 593.
[27] A.E. Karu and M. Beer, J. Appl. Phys. 37 (1965) 2179.
[28] P.W. Palmberg, R.E. De Wames, L.A. Vredevoe and T. Wolfram, J. Appl. Phys. 40 (1969) 1158.
[29] T. Suzuki, N. Hirota, H. Tanaka and H. Watanabe, J. Phys. Soc. Jpn. 30 (1971) 888.
[30] K. Katada, K. Nakahigashi and Y. Shimomura, Jpn. J. Appl. Phys. 9 (1970) 1019.
[31] B. Gale and K.F. Hale, Br. J. Appl. Phys. 12 (1961) 115.
[32] S.B. Fisher, Radiat. Eff. 5 (1970) 239.
[33] J. Verhoeven, Wang Wen-hao and J.J. Czyzewski, Surf. Sci. 143 (1984) 31.
[34] J. Finster, P. Lorenz, F. Fievet and M. Figrarz, Material Science Monographs, Vol. 10, Reactivity of Solids, Eds. Dyrek, J. Haber and J. Nowotny (Elsevier, Amsterdam 1982) p. 391.
[35] K.S. Kim and R.E. Davis, J. Electron Spectrosc. Relat. Phenom. (1972/73) 251.
[36] K.S. Kim and N. Winograd, Surf. Sci. 43 (1974) 625.
[37] P.C. Gravelles and S.J. Techner, Adv. Catal. 20 (1969) 168.
[38] F.P. Larkins and P.J. Fensham, Trans. Faraday Soc. 66 (1970) 1755.
[39] D. Brennen, D.O. Hayward and B.M.W. Trapnell, Proc. R. Soc. London A 256 (1960) 81.
[40] G.C. Word, I.G. Wright and J.M. Ferguson, Corros. Sci. 5 (1965) 645.
[41] D. Mekhandzhiev, Dokl. Bolg. Akad. Nauk. 22 (1969) 1253.
[42] P.W. Tasker and D.M. Duffy, Surf. Sci. 137 (1984) 91.